Supporting Information

Srinivasan et al. 10.1073/pnas.1110303108

SI Methods

Peptide Synthesis. Peptides derived from *Pf*RON2 were custom-synthesized by LifeTein LLC. Their sequences are listed in Fig. 2*B*. A biotin tag and a 6-carbon aminohexanoic acid (Ahx) linker were added to the N terminus. The thiol group in the cysteine side chains was blocked (by alkylation) according to proprietary methods (LifeTein LLC).

Ab Generation. Abs were generated against the RON2 peptide DIGAGPVASCFTTRMSPPQQICLNS(C) conjugated to KLH by introducing a C-terminal cysteine residue. Two rabbits were immunized with 0.5 mg of peptide per immunization with T-MAX adjuvant (Genscript USA) three times at 2-wk intervals and bled 2 wk after the third immunization. IgG from the two rabbits was affinity purified against the peptide immobilized to the Sulfolink coupling gel (GenScript USA). All IgGs were dialyzed against RPMI medium 1640 (KD Medical) before use in invasion inhibitory studies. The Ab was analyzed by Western blotting using merozoite extracts (Fig. S6*C*).

Ab Labeling for Confocal Microscopy. Cells were blocked overnight in 3% BSA, 0.1% Triton X-100 in PBS, pH 7.5, at 4 °C. The cells were centrifuged at 50 × *g* for 4 min at 4 °C. Primary Abs were diluted in the blocking solution, incubated for 2 h at room temperature, and washed three times with 1× PBS and 0.1% Triton X-100 at 50 × *g* for 4 min. Primary Abs used in this study were as follows: rabbit anti-AMA1, 1:400; rabbit anti-RON2 (1), 1:400; mouse anti-RON4 mAb 24C6 (2), 1:1,000; and anti-MSP1-33 mAb 1G3, 1:100. Samples were then incubated for 2 h with the corresponding secondary Abs (Alexa 488, Alexa 561, and Alexa 633), washed three times at 50 × *g* for 4 min, and mounted by using Prolong Gold containing DAPI (Invitrogen). The samples were allowed to polymerize overnight at 4 °C. Images were generated by using a Leica SP2 or a Zeiss 710 confocal microscope and visualized by using the Bitplane Imaris software.

Electron Microscopy. For transmission electron microscopy, following fixation, lysine was added to a final concentration of 50 mM, and samples were washed three times in 0.1 M phosphate buffer (pH 7.4) at room temperature and postfixed in 1% osmium tetroxide (Polysciences Inc.) for 1 h. Samples were then rinsed extensively in distilled water before en bloc staining with 1% aqueous uranyl acetate (Ted Pella) for 1 h. Following several rinses in distilled water, samples were dehydrated in a graded series of ethanol solutions and embedded in Eponate 12 resin (Ted Pella). Sections of 95 nm were cut with a Leica Ultracut UCT ultramicrotome, stained with uranyl acetate and lead citrate, and viewed on a JEOL 1200 EX transmission electron microscope.

For immuno-electron microscopy, following fixation, samples were washed three times in PBS at 4 °C, embedded in 10% gelatin, and infiltrated overnight with 2.3 M sucrose/20% poly(vinyl pyrrolidone) in Pipes–$MgCl_2$ at 4 °C. Samples were trimmed, frozen in liquid nitrogen, and sectioned with a cryo-ultramicrotome (Leica Microsystems). To detect RON4, sections were probed with mAb 24C6, followed by 18-nm colloidal gold-conjugated goat anti-mouse Ab (Jackson ImmunoResearch). Sections were stained with 0.3% uranyl acetate/2% methyl cellulose and viewed by transmission electron microscopy (Jeol USA).

Video Microscopy. Live video microscopy was performed by using a Leica SP2 microscope attached with a temperature- and CO_2-controlled incubator at 37 °C and 5% CO_2. Purified schizont-infected RBCs were mixed with RBCs warmed to 37 °C and observed for rupture and reinvasion. mAb 4G2 at a concentration of 1 mg/mL was used to study the effect of Abs on merozoite invasion.

Growth Inhibition Assay (GIA). Purified IgG at the desired concentration was dialyzed against RPMI 1640 (KD Medical). IgGs were incubated with O^+ human RBC to remove nonspecific Abs and incubated with *Pf*-parasitized RBC for 40 h. Parasitemia was quantified by biochemical measurement of *Pf* lactate dehydrogenase. All assays were performed in triplicate.

ELISA. Binding specificity of various peptides to AMA1 was performed according to a standardized ELISA protocol. Briefly, 96-well ELISA plates were coated with 100 ng/well of recombinant 3D7:00 AMA1 wild-type or Y251A protein at 4°C overnight in coating buffer (15 mM sodium carbonate and 35 mM sodium bicarbonate). The plates were blocked with diluent buffer consisting of 5% BSA (Sigma) in Tris-buffered saline (Cellgro) and 0.1% Tween 20 (TBS-T, pH 7.4). Dilutions of the various peptides (20 pmol each) in diluent buffer were added to antigen-coated wells in triplicate and incubated for 2 h at room temperature. Abs used for competition studies were mAb4G2 (0.5 μg per 100 μL) and mAb1F9 (0.25 μg per 100 μL). For recombinant AMA1 binding studies, we used anti-AMA1 rabbit IgG (0.5 μg per 100 μL), mAb4G2 (0.5 μg per 100 μL), and mAb1F9 (0.25 μg per 100 μL). All assays were carried out in triplicate. After washing the plates four times with TBS-T, the plates were incubated with alkaline phosphatase conjugated to streptavidin (Invitrogen) or the corresponding secondary Abs (Kirkegaard & Perry Laboratories) in blocking buffer for 2 h at room temperature. Binding was measured by adding *p*-nitrophenyl phosphate substrate (Sigma Chemical). The absorbance at 405 nm was read by using a SPECTRAmax 340PC microplate reader (Molecular Devices). For competition experiments, mAbs 4G2 (5 μg/mL) and 1F9 (2.5 μg/mL) were either preincubated with recombinant AMA1 for 1 h (preincub) before adding RON2L (20 pmol) or were mixed together simultaneously and incubated with recombinant AMA1. Rat mAb 4F2 recognizes the cytoplasmic tail of AMA1 and was used as a negative control.

^{35}S-Labeling of Parasite Proteins. Mature schizonts (5×10^7 per mL) were incubated in medium lacking Met and Cys and 200 μCi ^{35}S Met, Cys mixture and incubated at 37 °C. Labeled schizonts were collected after 3–4 h (before start of rupture), and saponin (0.1%) was lysed to release the parasites from RBC and washed in PBS. The pellet was resuspended in ice-cold parasite solubilization buffer [50 mM Tris·HCl, pH 7.5, 150 mM NaCl, 2 mM EDTA, 1% Triton X-100, and protease inhibitor mixture (Roche)]. The lysate was centrifuged at 15,000 × *g* for 30 min at 4 °C. The supernatant was used for pull-down analysis with anti-AMA1 Ab (5 μg) or RON2L peptide (5 μg). The complex was affinity purified by using anti-rabbit IgG or streptavidin-coated beads. After five washes in parasite solubilization buffer (pH 7.6), bound proteins were eluted in LDS loading buffer, run on 5–25% SDS/PAGE gels, transferred to a PVDF membrane, and exposed to X-ray film for the appropriate time to detect associated proteins. Parasite lysate from 5×10^7 schizont-infected RBCs was used for each pull-down.

Aldolase Pull-Down Assay. The amino acids corresponding to the C-terminal cytoplasmic tail of AMA1, TRAP, and the various mutations in the C-terminal tail of AMA1 and TRAP were synthesized with an N-terminal biotin tag and an Ahx linker

(Fig. 6). Each peptide (3 μg) was incubated with streptavidin beads (Invitrogen) in binding buffer (50 mM Tris·HCl, pH 7.5, 50 mM KCl, 0.2 mM EDTA, 1% BSA, and 0.1% Tween-20) for 1 h at room temperature. Unbound peptides were washed, and 15 μg of rabbit muscle aldolase (Sigma) in binding buffer was added to the peptide-bound beads and incubated for 4–8 h at 4 °C. For competition assays, 2 mM fructose-1,6-biphosphate (Sigma) was added along with 15 μg of aldolase. Beads were washed four times is wash buffer (50 mM Tris·HCl, pH 7.5, 50 mM KCl, 0.2 mM EDTA, and 0.2% Tween-20), and the bound complex was eluted in SDS loading buffer and analyzed on SDS/PAGE.

Modeling the AMA1–RON2L Complex. Creating a model for the RON2 peptide–AMA1 complex was done in a two-step process. In the first step, a tertiary model for the primary amino acid sequences of the RON2L peptide orthologs was generated based on in silico folding of the orthologous sequences. In the second step, the fit of the peptide to the hydrophobic cleft of AMA1 was evaluated computationally. The amino acid sequences for the six RON2L peptides from *Plasmodium* and *Toxoplasma* that are shown in Fig. S2*A* were folded in silico by using the Rosetta3 abrelax protocol (3). For each homologous peptide, 1,000 models were generated. During the simulations, the cysteines in the peptides were forced to adopt a disulfide bond. The 10 lowest energy models of each homologous peptide were structurally aligned with every other low energy model by using lsqman (4). A plot was generated from the 30 pairs of structural alignments with the lowest RMSDs (ranging from 3.2 to 5.1 Å), eight of which made up the largest cluster with the *Pf*RON2L model (Fig. S3*A*) at the center of that cluster.

A common fold was highly represented among the predicted structure for all seven homologous RON2L peptides. The fold consists of a short N-terminal helix and longer C-terminal helix, connected by a loop stabilized by disulfide bonds (Fig. S3). Deviations in the structural alignments between the models were found predominantly in the loop region. The majority of the residues conserved or partially conserved among the seven homologs map to the flat surface of the helical bundle distal to the loop.

The existing crystal structures of *Pf*AMA1 contain highly disordered loops adjacent to the hydrophobic pockets (5). Hence we used the existing crystal structure of *Tg*AMA1 (6) to model the AMA1–RON2L complex. *Tg*RON2L with the lowest energy model in the largest cluster from the folding simulation analysis was chosen for further modeling (Fig. S3*A*). The *Tg*RON2L model and *Tg*AMA1 crystal structure are complimentary in shape and electrostatics (Fig. S4*B*). Based on this observation, a starting model for the complex was created and subjected to the Rosetta3 FastRelax protocol (7). The final model obtained is the lowest energy model from 768 relax-trajectories. Electrostatic surface calculations were performed with APBS (8). During the simulation, the *Tg*RON2L peptide underwent a rigid body pivot movement about the C terminus of ∼3–4 Å, but the backbone did not change significantly (0.34 Å c-alpha RMSD). The majority of AMA1 did not change during the simulation (0.67 Å c-alpha RMSD over 336 residues); however, there were ∼2- to 3.5-Å movements in the loops surrounding the cleft. These regions correspond to the regions with the highest b factors in the crystal structure (Fig. S4*A*). All of the models were visualized by using PyMOL.

1. Cao J, et al. (2009) Rhoptry neck protein RON2 forms a complex with microneme protein AMA1 in Plasmodium falciparum merozoites. *Parasitol Int* 58:29–35.
2. Alexander DL, Arastu-Kapur S, Dubremetz JF, Boothroyd JC (2006) Plasmodium falciparum AMA1 binds a rhoptry neck protein homologous to TgRON4, a component of the moving junction in Toxoplasma gondii. *Eukaryot Cell* 5:1169–1173.
3. Raman S, et al. (2009) Structure prediction for CASP8 with all-atom refinement using Rosetta. *Proteins* 77(Suppl 9):89–99.
4. Kleywegt GJ, Jones TA (1999) Software for handling macromolecular envelopes. *Acta Crystallogr D Biol Crystallogr* 55:941–944.
5. Bai T, et al. (2005) Structure of AMA1 from Plasmodium falciparum reveals a clustering of polymorphisms that surround a conserved hydrophobic pocket. *Proc Natl Acad Sci USA* 102:12736–12741.
6. Crawford J, Tonkin ML, Grujic O, Boulanger MJ (2010) Structural characterization of apical membrane antigen 1 (AMA1) from Toxoplasma gondii. *J Biol Chem* 285: 15644–15652.
7. Tyka MD, et al. (2011) Alternate states of proteins revealed by detailed energy landscape mapping. *J Mol Biol* 405:607–618.
8. Baker NA, Sept D, Joseph S, Holst MJ, McCammon JA (2001) Electrostatics of nanosystems: Application to microtubules and the ribosome. *Proc Natl Acad Sci USA* 98:10037–10041.

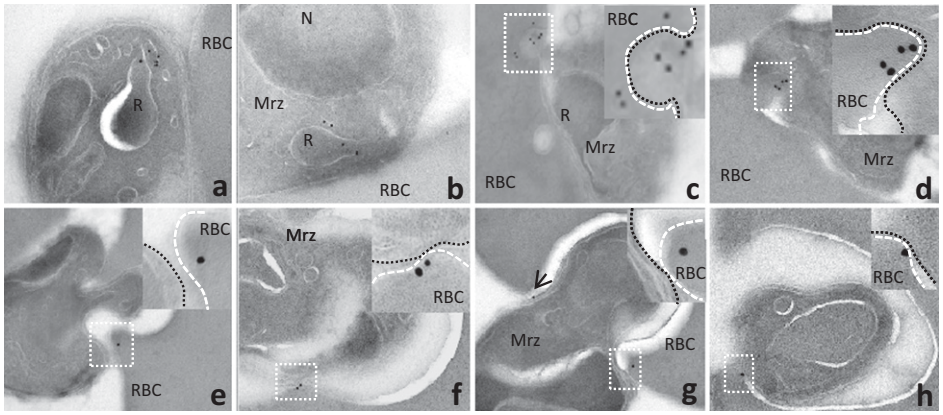

Fig. S1. *Pf*RON4 is secreted into the RBC before invasion and localizes at the moving junction on the cytoplasmic face of the RBC. Immuno-gold labeling of RON4 during merozoite invasion is shown. RON4 is localized within the rhoptry neck of an attached (I) and apically oriented merozoite (*B*). RON4 is secreted into the RBC early during invasion and is found both in the merozoite and RBC (*C*) and localizes at the moving junction predominantly facing the RBC cytoplasm at various stages of merozoite invasion (*D*–*H*). *Insets* are enlarged views of the area marked by the corresponding white dotted boxes. The dotted boxes shown in *E*–*H* identify the moving junction of invading merozoite. The white and black dotted lines in *Insets* mark the boundary of the RBC and merozoite, respectively. Arrow points to one gold particle at the junction between the RBC and merozoite. Mrz, merozoite; R, rhoptry; N, nucleus.

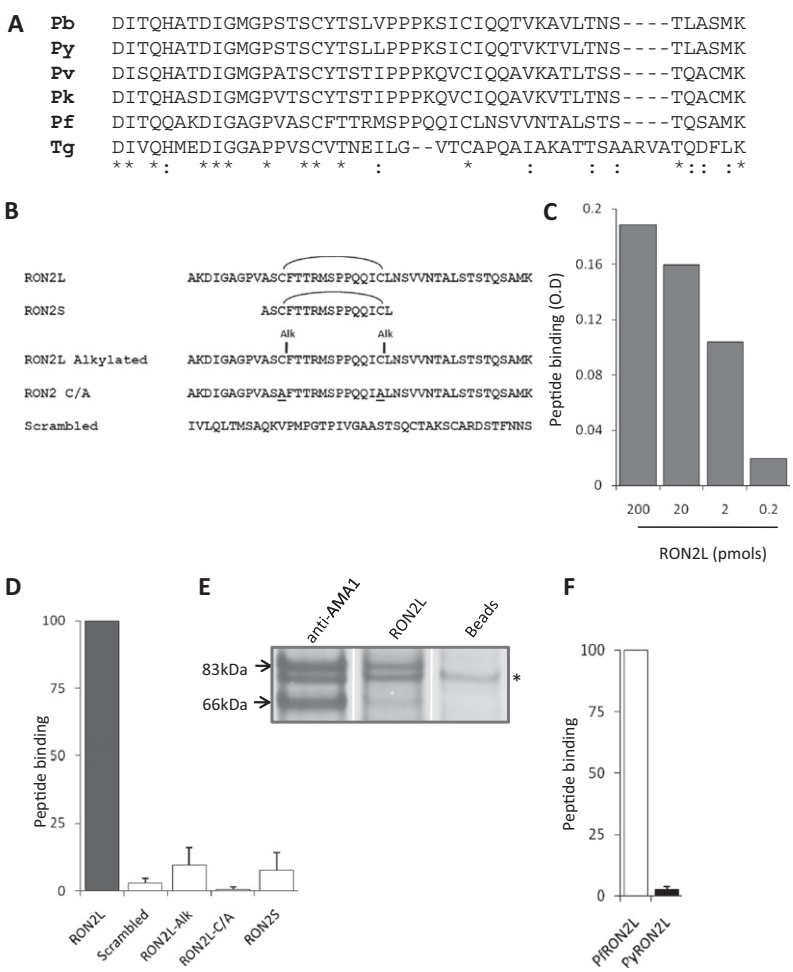

Fig. S2. Two conserved cysteine residues in RON2 are essential for binding AMA1. (*A*) Sequence alignment of the AMA1 binding region of RON2 (RON2L) among *Plasmodium* spp. and for *Tg*. *, identical residues. :, similar residues. (*B*) Peptide sequences of *Pf* RON2L and amino acid modifications used in this study. RON2L and RON2S peptides were synthesized with their two cysteine residues cyclized. All peptides were linked to biotin at their N terminus. (*C*) RON2L titration to determine optimal concentration for use in AMA1 binding assays. (*D*) The two central cysteine residues in RON2L are critical for binding AMA1. 20 pmol of the various peptides and 0.1 μg of recombinant 3D7:00 AMA1 were used in this ELISA. Results shown are pooled from two independent experiments done in triplicate, and data are represented as mean ± SEM. (*E*) Pull-down analysis of ^{35}S-labeled, triton-solubilized, schizont-infected RBC lysates was performed with anti-AMA1 polyclonal antisera (lane 1), RON2L peptide (lane2), or beads alone as control (lane 3). Identical results were obtained from an independent experiment. The arrows indicate the presence of the 83- and 66-kDa forms of AMA1. All of the lanes were from the same gel with the empty lanes removed (white line) for showing lanes side by side. * marks the nonspecific protein that binds to the beads. (*F*) PyRON2L does not bind PfAMA1. Results shown are pooled from two independent experiments done in triplicate, and data are represented as mean ± SEM. Pb, *Plasmodium berghei*; Py, *Plasmodium yoelli*; Pk, *Plasmodium knowlesi*; Pv, *Plasmodium vivax*. PlasmoDB accession nos.: Pb, PBANKA_131570 (residues 1,913–1,959); Py, PY06813 (residues 2,064–2,110); Pv, PVX_117880 (residues 2,035–2,081); Pk, PKH_125430 (residues 1,975–2,021); Pf(3D7), PF14_0495 (residues 2,021–2,067). *Tg*, GenBank accession no. HQ110093 (residues 1,293–1,346).

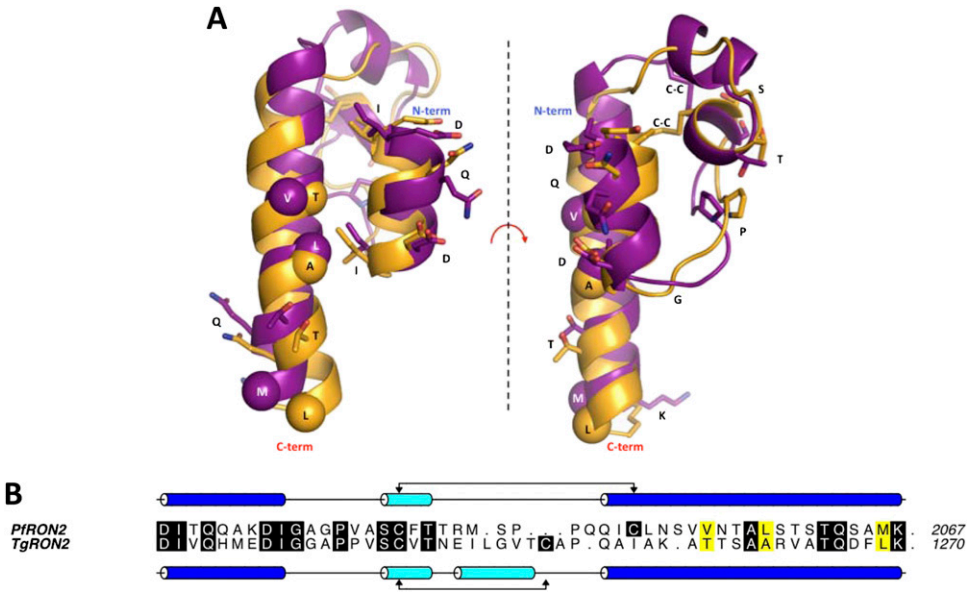

Fig. S3. Modeling the teritiary structure of *Pf* and *Tg* RON2L. (*A*) Superimposed models of the *Pf*RON2L (purple) and *Tg*RON2L (gold). The view on the right is a 90° rotation of the left view about the dashed line as shown by the arrow. Conserved amino acids are labeled and shown in stick representation. The c-alphas of hydrophobic amino acids in the C-terminal helix that are conserved among *Plasmodium* species are shown as spheres, and the amino acid types and disulfide bonds are labeled. Labels for residues that are obstructed in the views are omitted. (*B*) Sequence alignment of *Pf* and *Tg* RON2L based on the predicted model. Secondary structure of the corresponding region is indicated above and below the alignment. Predicted helices involved in forming the two-helix bundle are colored dark blue and the helices in the predicted loop region are colored cyan. The disulfide bonds are indicated by a line with connecting arrows. Black columns show conserved residues in the alignment. Note, the second cysteines do not structurally align however; they are colored black for clarity. Residues in the C terminus conserved among *Plasmodium* species are shown in the yellow columns. The colored residues in the alignment correspond to residues that are explicitly shown on the models.

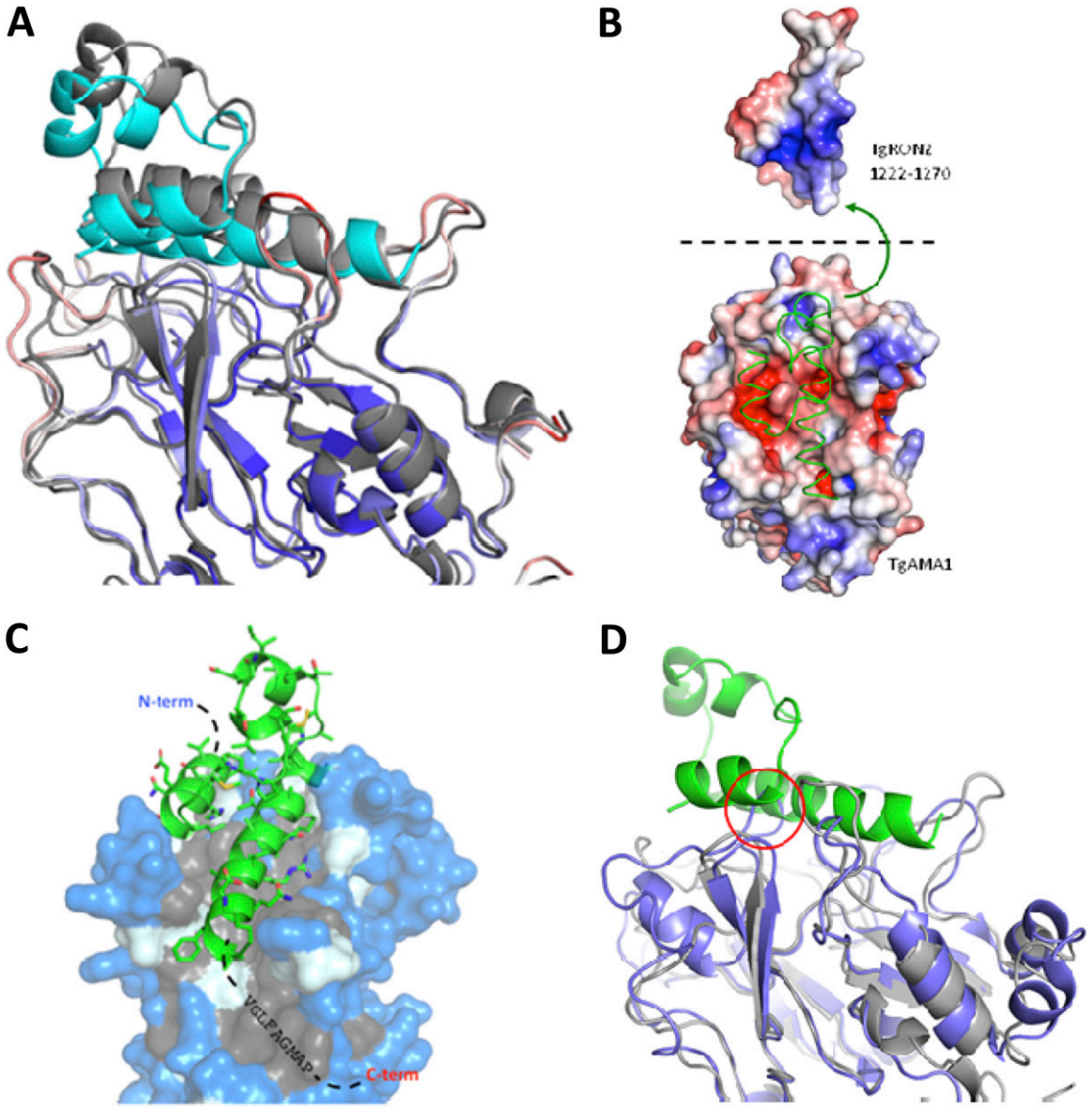

Fig. S4. Modeling *Tg*AMA1–*Tg*RON2L interaction. (*A*) *Tg*AMA1–RON2L model before (colored) and after (gray) complex simulation. Superimposition of the starting complex model with the *Tg*RON2L (cyan) in the hydrophobic groove of the *Tg*AMA1 crystal structure (red, white, and blue) and the final computational model (gray) illustrating the changes in position of the peptide and conformation of AMA1 that occurred during the simulation. In the starting model, the TgAMA1 crystal structure is colored by b-factor, varying from low (blue) to medium (white) to high (red). (*B*) Electrostatic potentials mapped to the solvent accessible surfaces of *Tg*AMA1 and *Tg*RON2 in the complex model. The complex is shown at the bottom looking down on the hydrophobic cleft. The *Tg*RON2 peptide is shown in green as a ribbon diagram. The *Tg*RON2L peptide is rotated 180 degrees around the axis represented by the green arrow and dashed line to show the *Tg*RON2 peptide surface that is in contact with the hydrophobic pocket of *Tg*AMA1 in the model. (*C*) Model of *Tg*AMA1–*Tg*RON2L complex showing the orientation of the peptide and highlighting the exposed hydrophobic patch of *Tg*AMA1 adjacent to the C terminus of the *Tg*RON2L. Amino acid residues in AMA1 are shown in gray (hydrophobic), blue (polar) and light cyan (all other residues). The sequence of nine amino acids following the C terminus of the RON2L is shown as an extension of the peptide. (*D*) Superimposition of *Pf*AMA1 (blue) over the *Tg*AMA1–RON2L complex model (gray and green, respectively) showing that domain II loop of *Pf*AMA1 overlaps in space (circled in red) with the RON2L peptide suggesting that this loop in *Pf* may play a role in binding RON2.

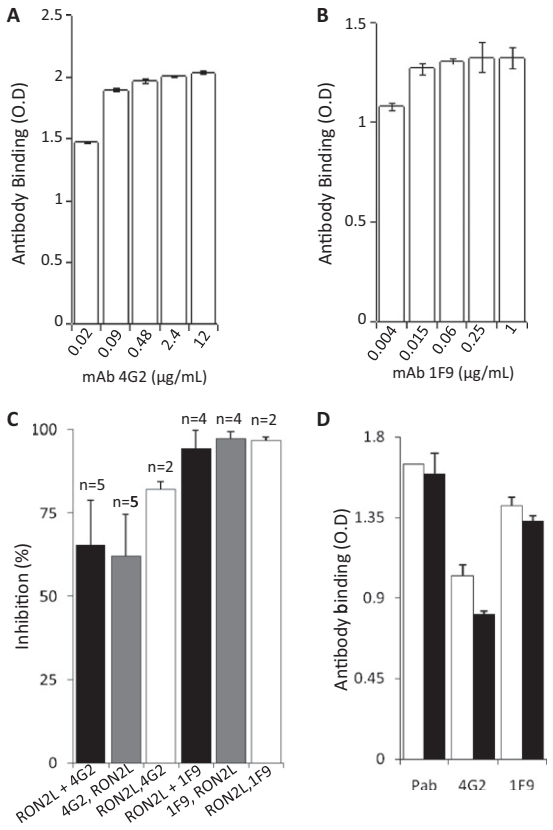

Fig. S5. RON2L binds the hydrophobic pocket of AMA1. (*A* and *B*) Titration of mAbs 4G2 and 1F9 to determine optimal concentration for use in RON2L inhibition ELISA. (*C*) mAbs 4G2 and 1F9 inhibit RON2L binding to AMA1 as well as displaces already bound RON2L. 20 pmol of RON2L, 5 μg/mL mAb 4G2, and 2.5 μg/mL mAb 1F9 were used in these assays. Peptide and Ab were either added together (RON2L+4G2 and RON2L+1F9) or were added one after the other (4G2,RON2L: 4G2 followed by RON2L; RON2L,4G2: RON2L followed by 4G2; 1F9,RON2L: 1F9 followed by RON2L; RON2L,1F9: RON2L followed by 4G2). Results shown are mean ± SEM from pooled data. Numbers above each bar (*n*) indicates the number of independent experiments. (*D*) Mutation of Tyr-251 does not affect the binding of conformation-dependent mAbs 4G2 and 1F9. Rabbit Abs to a combination of 3D7 and FVO recombinant AMA1 (Pab) are also unaffected by the mutation. Open and filled bars represent wild-type and Y251A recombinant AMA1, respectively. Results shown are pooled data from two independent experiments represented as mean ± SEM.

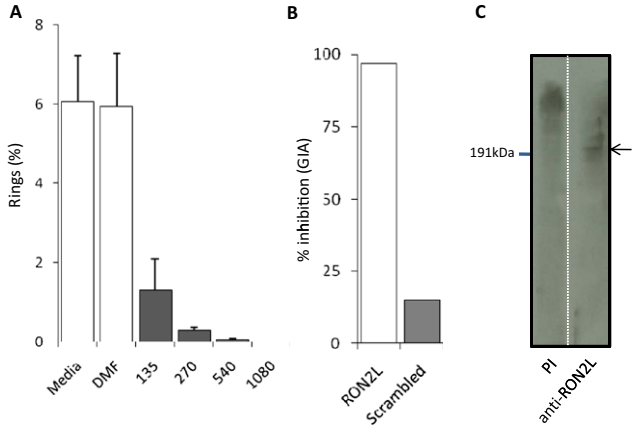

Fig. S6. RON2L peptide inhibits merozoite invasion of RBCs. (*A*) Purified merozoites (5×10^7) were mixed with prewarmed RBCs (2.5×10^7) in the presence of different concentrations (pmols) of RON2L and incubated at 37 °C for 30 min. Invasion efficiency was determined by counting newly formed rings in Geimsa staining. Medium or dimethyl formamide (DMF) were used as controls. (*B*) Invasion efficiency measured by growth inhibition assay (GIA). RON2L peptide or a scrambled peptide (540 pmol each) was used in a standard GIA. (*C*) Western blot analysis of anti-RON2L Ab using merozoite extract. A single predominant band of the correct size (black arrow) is recognized by anti-RON2L Ab but not the preimmune sera (PI). Dotted line is shown to indicate that the two sides of the blot were probed separately with the respective Abs.

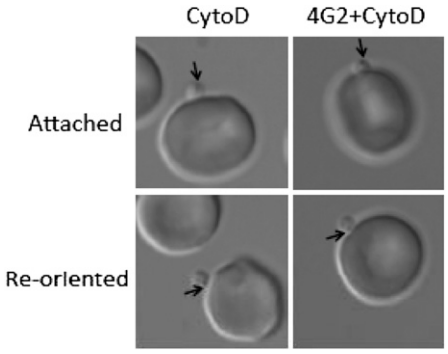

Fig. S7. mAb4G2 does not inhibit reorientation of the merozoite. Invasion inhibitory mAb 4G2 does not affect reorientation of cytochalasin D-treated merozoite (Table S1). Cytochalasin D (2 μM) treated merozoites with or without mAb 4G2 were allowed to bind prewarmed RBCs at 37 °C for 15 min. Parasites were fixed and observed under differential interference contrast microscopy. Orientation of the merozoites was determined by the presence of a dense protrusion at the apical end (arrows).

```
Pf EKYDKMDEPQ-D-YG--KSNSRN-DEMLDPEASFWGEEKRASH------TTPVLMEKPYY
Tg EH-E-F---QSDR-GARKK--RPSDLMQEAEPSFW-DE--AEENIEQDGETHV-MVEGDY
   :  : :   * :  *  *   *  *   : * *** ::  *         * * * :  *
```

Fig. S8. Sequence comparison of cytoplasmic tail of AMA1. Sequence alignment of *Pf* and *Tg* AMA1 cytoplasmic tail residues. Mutations in the residues analyzed in *Pf* (this study) and *Tg* (7) for binding aldolase are underlined. *, Identical residues; :, similar residues. *Pf*, PlasmoDB accession no. PF11_0344 (residues 574–622). *Tg*, GenBank accession no. AAB65410.1 (residues 494–541).

Table S1. Orientation of cytochalasin D-treated merozoites attached to RBCs

	Apical, %	Not apical, %	Total counted
Expt 1			
Control	83	17	35
4F2	78	22	41
4G2	74	26	39
Expt 2			
Control	57	43	28
4G2	59	41	32
Expt 1			
Control	69	31	29
RON2L	73	27	45
Expt 2			
Control	53	47	30
RON2L	80	20	25

Attachment and reorientation of merozoites is not affected by mAb 4G2 and RON2L peptide. mAb 4F2 that binds to the cytoplasmic tail of AMA1 was used as a rat mAb negative control.

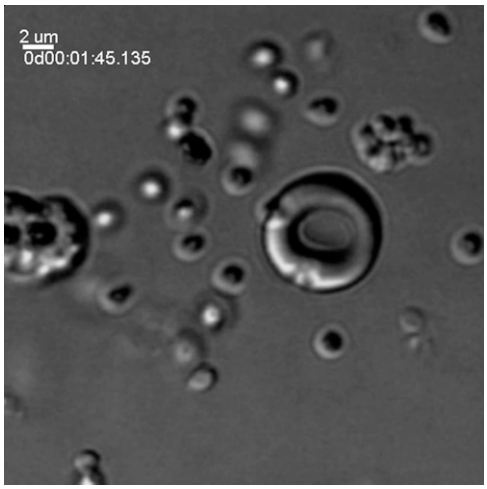

Movie S1. Live video microscopy of merozoite invasion. Normal schizont rupture and invasion of RBC by merozoites are shown.

Movie S1

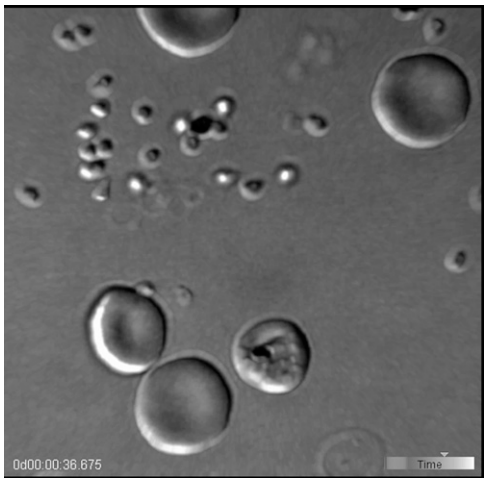

Movie S2. Live video microscopy of merozoite invasion in the presence of anti-AMA1 mAb 4G2. In the presence of invasion inhibitory mAb 4G2, the merozoite makes apical contact, but does not form the junction and, as a result, falls off the RBC.

Movie S2